

# AN EXTENDED MODEL FOR THE GROWTH AND COALESCENCE OF VOID - APPLICATION TO FRACTURE TOUGHNESS PREDICTION

T. PARDOEN\*, J.W. HUTCHINSON

Division of Engineering and Applied Sciences, Harvard University, Pierce Hall, Cambridge MA 02138, U.S.

\*also Université catholique de Louvain, Département des Sciences des Matériaux et Procédés, PCIM, Bâtiment Réaumur, 2 Place Sainte Barbe, 1400 Louvain-la-Neuve, Belgium. (pardoen@pcim.ucl.ac.be)

## ABSTRACT

An extended Gurson model incorporating the effects of the shape and spacing of the voids on the growth and coalescence is proposed. The onset of void coalescence is modeled as a transition from diffuse plasticity to transverse localized plastic yielding in the intervoid ligament. A simple constitutive model for the coalescence stage is also developed. Selected results are presented showing the importance of correctly accounting for the void coalescence stage, as well as for the void shape and distribution effects. The effect of the void shape on the fracture toughness is finally addressed using the assumption of uniaxial straining state of the fracture process zone. The analysis reveals that the effect of the void shape on the fracture toughness becomes significant for initial porosity larger than  $10^{-4}$  and this effect increases for increasing initial porosity.

## INTRODUCTION

Recent efforts in the development of computational models incorporating the void growth process has given rise to robust predictive methods for crack propagation in ductile solids, e.g. [1,2,3,4,5]. Most of these works employed the constitutive model initially proposed by Gurson [6], improved by Tvergaard [7], and finally extended by Needleman and Tvergaard [8]. Although good agreement with a range of experiments and void cells computations has been observed, the model as it currently stands still suffers from significant limitations:

- (i) The transfer of experimental data obtained from non-cracked specimens for the modeling of cracked structures, and vice-versa, is not yet successful. In order to quantitatively reproduce experimental  $J_R$  curves, parameters of the model must be identified by fitting to test data taken under high stress triaxiality conditions such as from a cracked specimen (e.g. [5]). Many problems of ductile fracture in non-cracked structures occur at low to intermediate stress triaxiality, e.g. during metal forming or in structures containing notches.
- (ii) In the context of the model as it now stands, non-spherical voids can only be accounted for in an ad hoc manner by introduction of an effective porosity.
- (iii) The phenomenological criteria currently employed to signal the onset of coalescence are limited to a restricted range of conditions, which are not easily measured experimentally.

These limitations, and others, are thought to arise mainly because (i) *void shape* is not directly accounted for and (ii) *void coalescence* is not properly modeled. The objective of the present paper is to describe a realistic model which would represent a step towards attainment of a complete model for failure due to the ductile failure mechanism of void nucleation, growth and coalescence. Selected results showing significant void shape and spacing effects or emphasizing the importance of a sound void coalescence model (i.e. cases where simpler model like critical porosity models completely miss the point) are examined in order to

motivate the necessity for such an enhanced model. It is important to mention that all the results presented here are all in close agreement with more exact void cell prediction [9]. At the end of the paper, the fracture toughness of ductile materials with preferentially orientated non-spherical inclusion is addressed by invoking the approximation of uniaxial straining for the crack tip stress state.

## EXTENDED MODEL FOR THE GROWTH AND COALESCENCE OF VOIDS

We have borrowed heavily from two contributions in the literature, and have integrated them into the enhanced model. The first contribution is the model of Gologanu-Leblond-Devaux [10], extending the Gurson model to void shape effects. Indeed, it will be shown that void shape effects must be accounted for in order to correctly predict the ductility at small stress triaxiality. The second is the approach of Thomason [11] for the onset of void coalescence. Each of these has been extended heuristically to account for strain hardening. In addition, a micromechanically-based simple constitutive model for the void coalescence stage is proposed to supplement the criterion for the onset of void coalescence. Only axisymmetric stress states are considered in the present work and the solid is made of a periodic distribution of the cylindrical representative volume element (RVE) defined on Fig. 1.

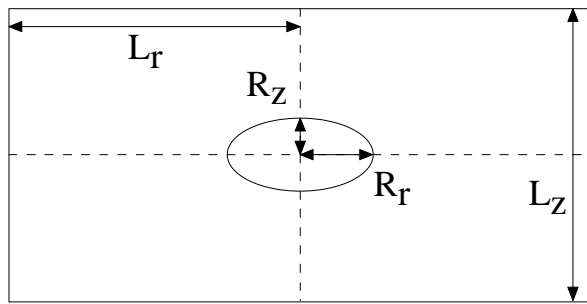


**Figure 1.** Representative volume element.

**Void growth model.** The extension of the Gurson model due to Gologanu *et al.* [10], which has been adopted here to describe behavior prior to void coalescence, gives a constitutive relation for a porous elastoplastic material containing (axisymmetric) spheroidal voids. This particular model, extended for strain-hardening, contains as state variables: the components of the mesoscopic stress tensor,  $\Sigma$ , the porosity,  $f$ , the void aspect ratio,  $S$ , and an average yield stress for the matrix material,  $\sigma_m$ . The void aspect ratio is defined by  $S = \ln(W)$  while  $W = R_z/R_r$ . The functional form of model prior to coalescence is:

$$\Phi \equiv \Phi(\Sigma, f, S, \sigma_m) = 0, \quad (1)$$

$$\dot{f} = (1 - f) \dot{E}_{kk}^p, \quad (2)$$

$$\dot{S} \equiv \dot{S}(f, S, T), \quad (3)$$

$$\sigma_m \dot{\epsilon}_m^p (1 - f) = \sum_{ij} \dot{E}_{ij}^p, \quad (4)$$

$$\sigma_m \equiv \sigma_m(\epsilon_e), \quad (5)$$

$$\dot{E}_{ij}^p = \gamma \frac{d\Phi}{d \Sigma_{ij}}, \quad (6)$$

where  $\Phi$  is the flow potential;  $E^p$  is the mesoscopic plastic strain tensor; (2) and (3) are the evolution laws for  $f$  and  $S$ , respectively; (4) is the Gurson [6] energy balance for the plastic work allowing computation of  $\sigma_m$  using the effective stress-strain curve for the parent material (5); and (6) is the flow rule. The structure of the original Gurson model has been retained. The expressions for the functions such as  $\Phi$  and the evolution of  $S$  are given in Ref. [9,10].

**Criterion for the onset of void coalescence.** Axisymmetric void cell computations [9,12] have shown that void coalescence consists in the localization of plastic deformation in the ligament between the voids, which, experimentally, gives rise to a flat dimpled fracture surface. (Void coalescence by shear localization is also observed in other states of stress [7], but, up to now, our model is limited to tensile localization.) Thomason [11] has studied the transition to localization for elastic-perfectly plastic solids by looking at artificially constrained localized solutions giving the load as a function of the void cell geometry. The relation between the overall tensile stress  $\Sigma_z/\sigma_0$  and the overall strain  $E_z$  based on the full cell length is sketched qualitatively in Fig. 2. At low overall strain (small porosity),  $\Sigma_z/\sigma_0$  required for localized yielding is far greater than the actual value from the cell. However, the actual solution peaks and falls (with the cell still deforming in a diffuse manner) until localization sets in, and then the actual solution merges with the artificially constrained localized solution which is significantly affected by the growth of the void. This is the transition point, and from this point on, the solution is localized within the ligament.

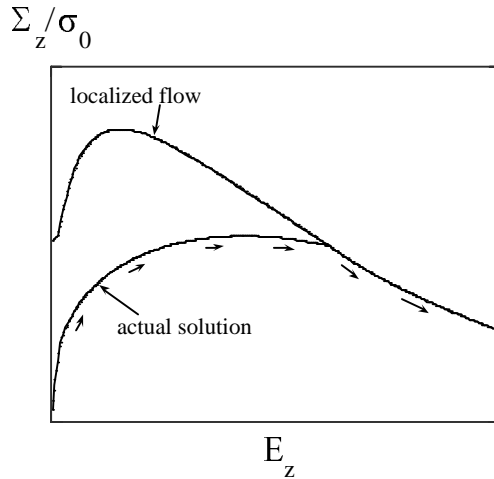


**Figure 2.** Qualitative sketch of the axial stress vs axial strain curves predicted by the constrained localized solution and by the full cell solution; the transition to localization sets in when the solution for diffuse plasticity merges with the solution for a localized plastic flow.

For axisymmetric geometries, Thomason has proposed that the average normal stress acting on the cell at the onset of localization occurs when  $\Sigma_z$  attains  $\Sigma_z^{loc}$  where

$$\frac{\Sigma_z^{loc}}{\sigma_0} = \left[ 1 - \left( \frac{R_r}{L_r} \right)^2 \right] \left[ \alpha \left( \frac{R_z}{L_r - R_r} \right)^{-2} + \beta \left( \frac{R_r}{L_r} \right)^{-\frac{1}{n}} \right], \quad (7)$$

where  $\alpha = 0.1$  and  $\beta = 1.2$ . By comparing this expression with our numerical results for strain hardening materials, we also find that this expression provides an accurate estimate for the onset of localization within the cells, provided that  $\sigma_0$  is replaced by an appropriate effective flow stress for the matrix,  $\sigma_m$  (see also [13]), and  $\alpha$  and  $\beta$  incorporate a dependence on the strain hardening exponent  $n$ . The effective matrix stress,  $\sigma_m$ , is obtained using (4) and (5). Thus, with attention confined to cases where  $\Sigma_z$  is the maximum principal stress, localization is assumed to set in when  $\Sigma_z = \Sigma_z^{loc}$  where

$$\frac{\Sigma_z^{loc}}{\sigma_m} = \left[ 1 - \left( \frac{R_r}{L_r} \right)^2 \right] \left[ \alpha(n) \left( \frac{R_z}{L_r - R_r} \right)^{-2} + \beta(n) \left( \frac{R_r}{L_r} \right)^{-\frac{1}{2}} \right]. \quad (8)$$

A fitting procedure performed on a large number of void cell results [9] has revealed that the coefficient  $\beta$  is almost constant equal to 1.24 while

$$\alpha(n) = 0.1 + 0.217n + 4.83n^2 \quad (0 \leq n \leq 0.3), \quad (9)$$

With relations (7) or (8), a new geometrical variable related to the void spacing has entered the model. For the sake of simplicity in the formulation of the model, we have chosen to use  $A = \ln(\lambda) = \ln(L_z/L_r)$ . The model thus depends on all the geometric characteristics of the representative void cell:  $f$ ,  $A$  (or  $\lambda$ ),  $S$  (or  $W$ ). In [9], the criterion (8) has proved to predict the onset of coalescence with a very high degree of accuracy for porosities ranging between  $10^{-2}$  and  $10^{-4}$ , stress triaxialities between 1/3 and 5, void shapes  $W$  between 1/6 and 6, and void distribution  $\lambda$  between 1/2 to 16.

**A model for the post-localization regime.** Relation (8) still pertains after the onset of coalescence and  $\Sigma_z^{loc}$  is replaced by  $\Sigma_z$ , assuming the voids do not depart significantly from a spheroidal shape. The additional equations for the evolution of the state variables during the post-localization stage are obtained under the approximation that elasticity, as well as any reversed plasticity, are neglected. In agreement with the void cell results, the half-height of the localization zone is approximated as  $R_z$  (i.e.  $h = R_z$ , see Fig. 1). Plastic incompressibility still implies (2) for the evolution of  $f$  and the evolution of  $A$  is also elementary:

$$\dot{A} = \dot{E}_z. \quad (10)$$

The evolution of  $S$  can be determined by differentiating  $\ln(R_z/R_r)$ .

$$\dot{S} = \frac{3}{2} \left( \left( \frac{2 \exp(2(A-S))}{3f} \right)^{1/3} - \frac{1}{3f} \right) \dot{E}_z \quad (11)$$

In order to evaluate the average yield stress  $\sigma_m$  for the material in the localized band, the average strain rate  $\dot{\varepsilon}_e^{loc}$  is needed. This is obtained from the evolution of the localized band height as

$$\dot{\varepsilon}_e^{loc} = \frac{\dot{h}}{h} = \frac{\dot{R}_z}{R_z} = \left( \frac{2 \exp(2(A-S))}{3f} \right)^{1/3} \dot{E}_z. \quad (12)$$

## SELECTED RESULTS

**Void shape effect on coalescence at small stress triaxiality.** Fig. 3 shows the variation of the axial overall stress as a function of the overall axial strain for three different small stress triaxialities,  $T = \Sigma_h/\Sigma_e = 1/3, 2/3$  and 1 and three different initial void shapes,  $W_0 = 1/6, 1, 6$ . Void coalescence is detected by a sudden change of slope in the curves. At  $T = 1/3$ , a transition to a localized mode of yielding in the ligament is predicted to develop for the oblate ( $W_0 = 1/6$ ) void and not for the two other void shapes. For initially spherical or prolate voids, the porosity increases slightly at the beginning of the straining and then saturates to a maximum value for further straining. The void shape effect on the ductility is also very significant at  $T = 2/3$  and 1. For larger stress triaxiality ( $T > 2$ ), ductility does not depend much on the shape.

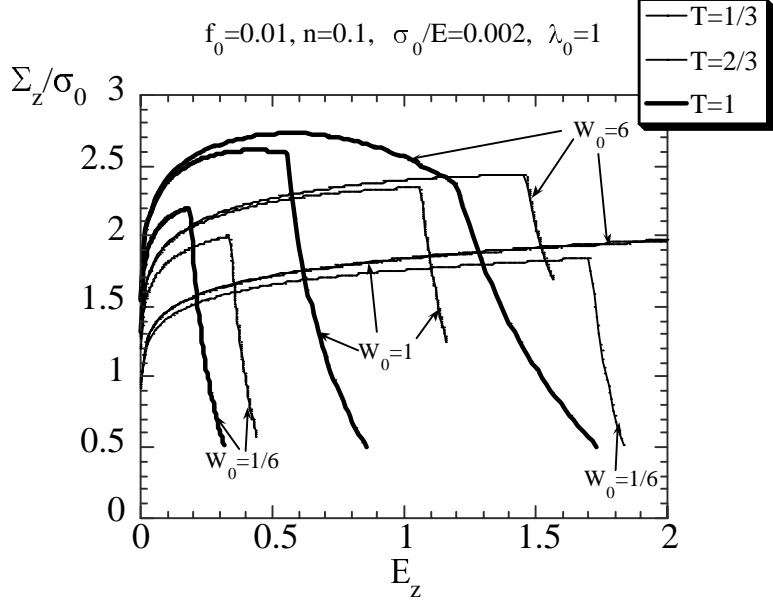


**Figure 3.** Predictions obtained with the void growth - void coalescence model for  $f_0 = 10^{-2}$ ,  $\lambda_0 = 1$ ,  $\sigma_0/E = 0.002$ ,  $n = 0.1$  and  $W_0 = 1/6, 1, 6$ , at  $T = 1/3, 2/3, 1$ ; overall axial stress vs overall axial strain.

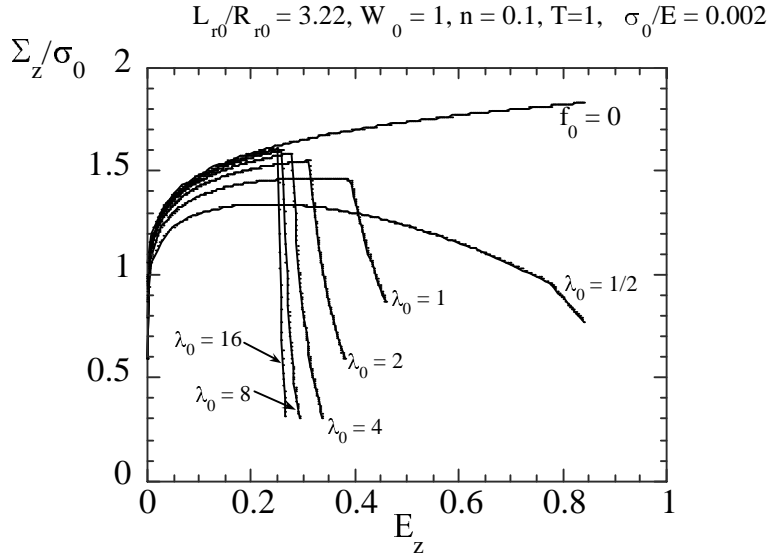


**Figure 4.**  $\Sigma_z$  vs  $E_z$  curves for  $n = 0.1$ ,  $W_0 = 1$ , a constant  $L_{r0}/R_{r0}$  ratio equal to 3.22, and  $T = 1$  (a) or  $T = 3$  (b), showing the effect of the cell aspect ratio.

**Void distribution effects on void coalescence.** The effect of the initial cell aspect ratio  $\lambda_0$  on void coalescence is depicted in Fig. 4 which presents  $\Sigma_e$  vs  $E_e$  for  $n = 0.1$ ,  $W_0 = 1$ ,  $T = 1$ , and the void spacing,  $L_{r0}/R_{r0}$ , fixed at 3.22. The true stress - true strain curve of the matrix material is also plotted ( $f_0 = 0$ ). The peak stresses converge to a well-defined point on the curve corresponding to  $f_0 = 0$  as  $\lambda_0$  increases. The limit,  $\lambda_0 \rightarrow \infty$ , corresponds to a single plane of voids in an infinite solid. For  $\lambda_0 = 16$ , the porosity is so small that there is nearly no departure from the curve  $f_0 = 0$  prior to localization. The transition to a uniaxial straining mode is observed for all values of  $\lambda_0$ . For large  $\lambda_0$ , the onset of void coalescence coincides with the peak stress, which, consequently, is due to the onset of the void coalescence localization process and not due to the competition between the hardening of the matrix and the softening due to void growth. The slope of the curve after the onset of void coalescence increases with  $\lambda_0$  as a result of an increasingly larger zone of elastic unloading. In Ref. [9], all the results presented here were found to be in close agreement with more exact void cell computations.

## FRACTURE TOUGHNESS PREDICTION

As initially proposed by Andersson [14] and then revisited by Tvergaard and Hutchinson [15], the fracture process zone can be anticipated as a row of multiple interacting voids which, to a good approximation, are strained uniaxially during the major part of the void growth. Indeed, under large stress triaxiality, the fracture process involves early localization of the plastic flow in a planar zone of essentially one void spacing in thickness. Assuming spherical voids and isotropic void distribution, Tvergaard and Hutchinson [15] have shown that the fracture toughness,  $J_{lc}$ , governing crack growth initiation can be expressed as

$$J_{lc} = \Gamma_0 \quad (13)$$

where  $\Gamma_0$  is the work per unit area spent in the band until final failure. It can be computed from the Gurson model according to

$$\frac{\Gamma_0}{\sigma_0 L_{r0}} = F\left(\frac{\sigma_0}{E}, n, f_0\right) \quad (14)$$

where  $v$  is the Poisson ratio and  $E$  is the Young's modulus.

Xia and Shih [16] and Tvergaard and Hutchinson [17] have shown that the uniaxial straining assumption is valid as long as  $f_0$  is not too small. Typically, when  $f_0$  becomes smaller than 0.1%, a one void - crack interaction mechanism takes place, as analyzed by Rice and Johnson [18] and also discussed in Tvergaard and Hutchinson [17]. In that case, the uniaxial straining assumption loses its pertinence. Furthermore,  $J_{IC}$  is not equal to  $\Gamma_0$  anymore because the fracture process zone is then embedded in the finite strain zone (a full analysis is required to relate  $\Gamma_0$  with the far field  $J$ ). Nonetheless, as long as the stress triaxiality is large enough, the  $\Gamma_0$  predicted by the uniaxial straining assumption for low porosity remains a good approximation of the exact  $\Gamma_0$  (although they are not equal to  $J_{IC}$ ). Indeed, at large stress triaxiality (typically,  $T > 2.5$ ), the overall stress-strain curve does not depend much on the stress triaxiality [19].

The analysis of Tvergaard and Hutchinson [15] has been extended by accounting for the effect of the void shape using the extended-Gurson model. Now,  $F$  generally writes

$$F = F\left(\frac{\sigma_0}{E}, n, f_0, W_0\right) \quad (15)$$

assuming isotropic initial void distribution ( $\lambda_0 = 1$ ). This extended model allows addressing the anisotropic fracture toughness of metal alloys formed by rolling, die-extrusion, or deep drawing. Indeed, since it accounts for the void shape, this model is able to capture variations of the fracture toughness with the orientation of the crack plane resulting from preferential orientation of the inclusions (e.g. [20]).

The variation of  $\Gamma_0/\sigma_0 L_{r0}$  as a function of the initial porosity for various void shapes is shown in Fig. 5 (for  $n = 0.2$  and  $\sigma_0/E = 0.002$ ). The effect of the initial void shape is significant for porosity larger than about  $10^{-4}$ . Prolate shape increases  $\Gamma_0/\sigma_0 L_{r0}$  while oblate shape reduces it. For void shape departing from spherical,  $\Gamma_0/\sigma_0 L_{r0}$  cannot be considered as independent of the initial porosity (as shown in Ref. [15] for spherical voids), it increases with  $f_0$  for prolate voids and decreases with  $f_0$  for oblate voids. The asymptote for prolate voids corresponds to a limit porosity at which the void touches the upper and lower parts of the cell. For oblate voids, the limit porosity results from that the void boundary is in contact with the lateral sides of the cell. In that case,  $\Gamma_0/\sigma_0 L_{r0} = 0$  because there is no more loading carrying capacity. Using straightforward geometrical relationships, these two limit porosity expresses as:

$$f_{0limitprolate} = \frac{2}{3} \frac{\lambda_0^2}{W_0^2} \quad \text{and} \quad f_{0limitoblate} = \frac{2}{3} \frac{W_0}{\lambda_0} \quad (16)$$

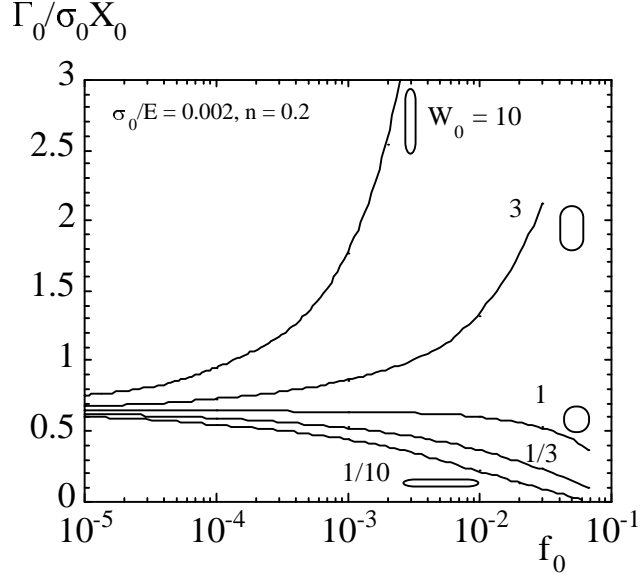


**Figure 5.** Variation of  $F = \Gamma_0/\sigma_0 X_0$  as a function of the initial porosity  $f_0$  for various initial void shape.

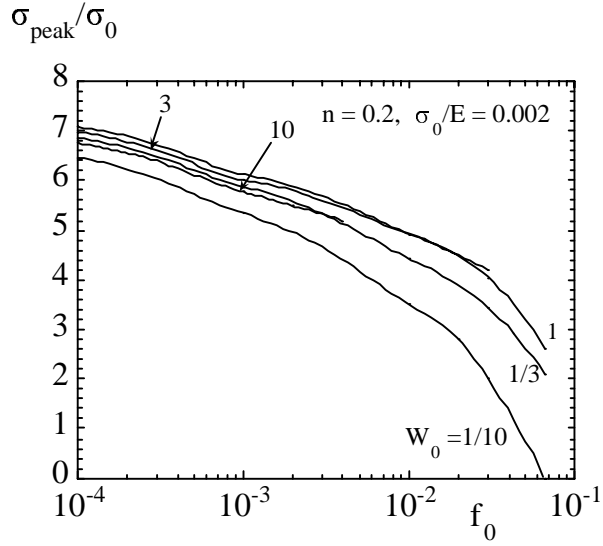


**Figure 6.** Variation of  $\sigma_{peak}/\sigma_0$  as a function of the initial porosity  $f_0$  for various initial void shape.

The results of Fig. 5 can be used to qualitatively understand and predict the variation of the fracture toughness as a function of the loading direction for rolled plates with preferential orientation of the second phase. One can consider that void shape effects can alone explain a factor two in the toughness of steel plates with elongated MnS inclusions. This analysis is only qualitative because of the assumed axisymmetry. In other words, a 90° rotation of a prolate void with  $W_0 = a$  does not give an oblate void with  $W_0 = 1/a$ .

The maximum stress attained in the cell is the other crucial parameter of the fracture process. It mainly affects the resistance to crack propagation [15], also called the "R-curve" effect. Fig. 6 shows that the maximum stress is not much affected by prolate shape while it decreases as the voids are more and more oblate. Oblate void shape is thus expected not only to bring about a decrease of the fracture toughness but also of the tearing resistance during crack propagation. One also notices that a spherical void shape ( $W_0 = 1$ ) brings about the maximum peak stress. More results are given and discussed in Ref. [21].

## CONCLUDING REMARKS

The new model only depends on the initial values of the state variable and thus avoids the use of critical porosities (for the onset of coalescence and for final separation). The two additional microstructural characteristics of the new model,  $S_0$  and  $\lambda_0$ , can be obtained from the same metallographic analysis performed to ascertain  $f_0$  and  $L_0$ . At large stress triaxiality (not discussed here), the work spent during the coalescence stage can be larger than the work spent during the void growth stage. This observation gives another motivation for the development of a constitutive model valid after the onset of localization. The comparison with the void cell simulations in Ref. [9] has established that the full void growth/coalescence model is able to quantitatively account for variations of all the characteristic parameters of the representative volume element of Fig. 1: porosity, void shape, cell aspect ratio, stress triaxiality, for a wide range of matrix flow behavior. The criterion for the onset of coalescence has been shown to be very accurate for most of the cases analyzed in this work. Most importantly, behavior at low and large stress triaxiality are adequately encompassed by the same model. The void shape effect on the fracture toughness due to the preferential orientation of second phases may alone explain the toughness anisotropy observed in many formed plates or bars.

## ACKNOWLEDGEMENTS

T.P. acknowledges a fellowship from the Fonds National de la Recherche Scientifique (F.N.R.S.) Belgium, and postdoctoral fellowships from the Belgian American Educational Foundation Inc. (B.A.E.F.) and from the Université catholique de Louvain (U.C.L.). The work of JWH was supported in part by the NSF grant CMS-9634632 and in part by the Division of Engineering and Applied Sciences, Harvard University.

## REFERENCES

1. Mudry, F., di Renzo, F., and Pineau, A., (1989). In: *Non-Linear Fracture Mechanics: Volume II - Elastic-Plastic Fracture*, ASTM STP 995, pp. 24-39, Landes, J.D., Saxena, A., and Merkle, J.G. (Eds). American Society for Testing and Materials, Philadelphia.
2. Xia, L., Shih, C.F., and Hutchinson, J.W. (1995). *J. Mech. Phys. Solids* **43**, 389.
3. Brocks, W., Klingbeil, D., Kunecke, G., and Sun, D.-Z. (1995). In: *Constraint Effects in Fracture Theory and Applications: Second Volume*, ASTM STP 1244, pp. 232-252, Kirk, M. and Bakker, A. (Eds). American Society for Testing and Materials, Philadelphia.
4. Ruggieri, C., Panontin, T.L., and Dodds, R.H., Jr. (1996). *Int. J. Fract.* **82**, 67.
5. Gao, X., Faleskog, J., and Shih, C.F. (1998). *Int. J. Fract.* **89**, 374.
6. Gurson, A.L. (1977). *J. Engng. Mater. Tech.* **99**, 2.
7. Tvergaard, V. (1981). *Int. J. Fract.* **17**, 389.
8. Needleman, A. and Tvergaard, V. (1984). *J. Mech. Phys. Solids* **32**, 461.
9. Pardoen, T. and Hutchinson, J.W. (2000) *J. Mech. Phys. Solids* in press.
10. Gologanu, M., Leblond, J.-B., Perrin, G., and Devaux, J. (1995). In: *Continuum Micromechanics*, Suquet, P. (Ed.). Springer-Verlag.
11. Thomason, P.F. (1990) *Ductile Fracture of Metals*, Pergamon Press, Oxford.
12. Koplik, J. and Needleman, A. (1988). *Int. J. Solids Struct.* **24**, 835.
13. Zhang, Z. L. and Niemi, E. (1994). *Engng. Fract. Mech.* **48**, 529.
14. Andersson, H. (1977). *J. Mech. Phys. Solids* **25**, 217.
15. Tvergaard, V. and Hutchinson, J.W. (1992) *J. Mech. Phys. Solids* **40**, 1377.
16. Xia, L. and Shih, C.F. (1995). *J. Mech. Phys. Solids* **43**, 1953.
17. Tvergaard, V. Hutchinson, J.W. (1996). *Int. J. Solids Struct.* **33**, 3297.
18. Rice, J.R. and Johnson, M.A. (1970). In *Inelastic Behavior of Solids*, Kanninen, M.F., Adler, W.F., Rosenfield, A.R., and Jaffee, R.I. (Eds.). McGraw-Hill, 641.
19. Siegmund, T. and Brocks, W. (1999). *Int. J. Fract.* **99**, 97.
20. Bauvineau, L. (1996). *Approche Locale de la Rupture Ductile: Application à un Acier Carbone-Manganèse*. Ecole Nationale Supérieure des Mines de Paris, Paris.
21. Pardoen, T. and Hutchinson, J.W., in preparation.